Supporting information

Re-Radiation Enhancement in Polarized Surface Enhanced Resonant Raman Scattering of Randomly Oriented Molecules on Self-Organized Gold Nanowires

Barbara Fazio,[a] Cristiano D'Andrea,[a] Francesco Bonaccorso,[a,] Alessia Irrera,[a] Giuseppe Calogero,[a] Cirino Vasi,[a] Pietro Giuseppe Gucciardi,[a,#] Maria Allegrini,[b] Andrea Toma,[c,§] Daniele Chiappe,[c] Christian Martella,[c] Francesco Buatier de Mongeot[c]*

[(a)] CNR IPCF Istituto per i Processi Chimico-Fisici, Viale F. Stagno D'Alcontres 37, I-98156, Messina, Italy

[(b)] Dipartimento di Fisica "Enrico Fermi", Università di Pisa and INO-CNR Sezione di Pisa, Largo Bruno Pontecorvo 3, 56126 Pisa, Italy

[(c)] Dipartimento di Fisica, Università di Genova, and CNISM, Via Dodecaneso 33, I-16146 Genova, Italy

* Present address: Department of Engineering, University of Cambridge, Cambridge CB3 0FA, United Kingdom.

[§] Present affiliation: Nanobiotech Facility, Istituto Italiano di Tecnologia, via Morego 30, Genova, I-16163, Italy.

[#] Corresponding author: gucciardi@me.cnr.it

1. Advantages of Ion Beam Sputtering

In Ion Beam Sputtering (IBS) a defocused ion beam destabilizes an otherwise flat surface, dislocating mobile adatoms and vacancies which re-arrange themselves *via* thermally activated diffusion, finally producing an array of periodic nano-structures (ripples, mounds, pyramids) which select a preferential periodicity (10nm – 500nm range).[1,2] The periodicity and orientation of the nanostructures is determined by the competition between a smoothing term (thermally activated diffusion) and a roughening term (erosive action of the ion beam). IBS is a fast and cost-effective method to sculpt surfaces at the nanometers scale and shows the ability to induce functional modification of the substrate, e.g. for tailoring chemical reactivity of magnetic anisotropy catalytic applications. IBS is a clean technique with respect to chemical synthesis methods,[3,4] cheaper and easier to implement with respect to electron beam lithography.[5] It is a single maskless process, which does not require solution based steps, being intrinsically contaminant-free and directly compatible for use in advanced spectroscopy and sensing. IBS can be applied for the production of new plasmonic materials with tunable anisotropic optical properties in the visible range and is a potential new tool to fabricate large area (cm^2) Surface Enhanced Raman Spectroscopy (SERS) - active substrates with engineered optical response. [6,7,8] By acting on ion energy, ion flux, ion dose, incidence angle, and substrate temperature, it is possible in fact to modify the morphological parameters of the nanostructures such as the lateral periodicity, facet slope, orientation and degree of connection (the minimum film thickness between adjacent Nanowires, NWs), and therefore the Plasmon resonance energy. Finally, IBS yields quite homogeneous samples of aligned NWs which are of great interest in applications where both the polarization of the SERS pump and that of emitted signal becomes an issue.

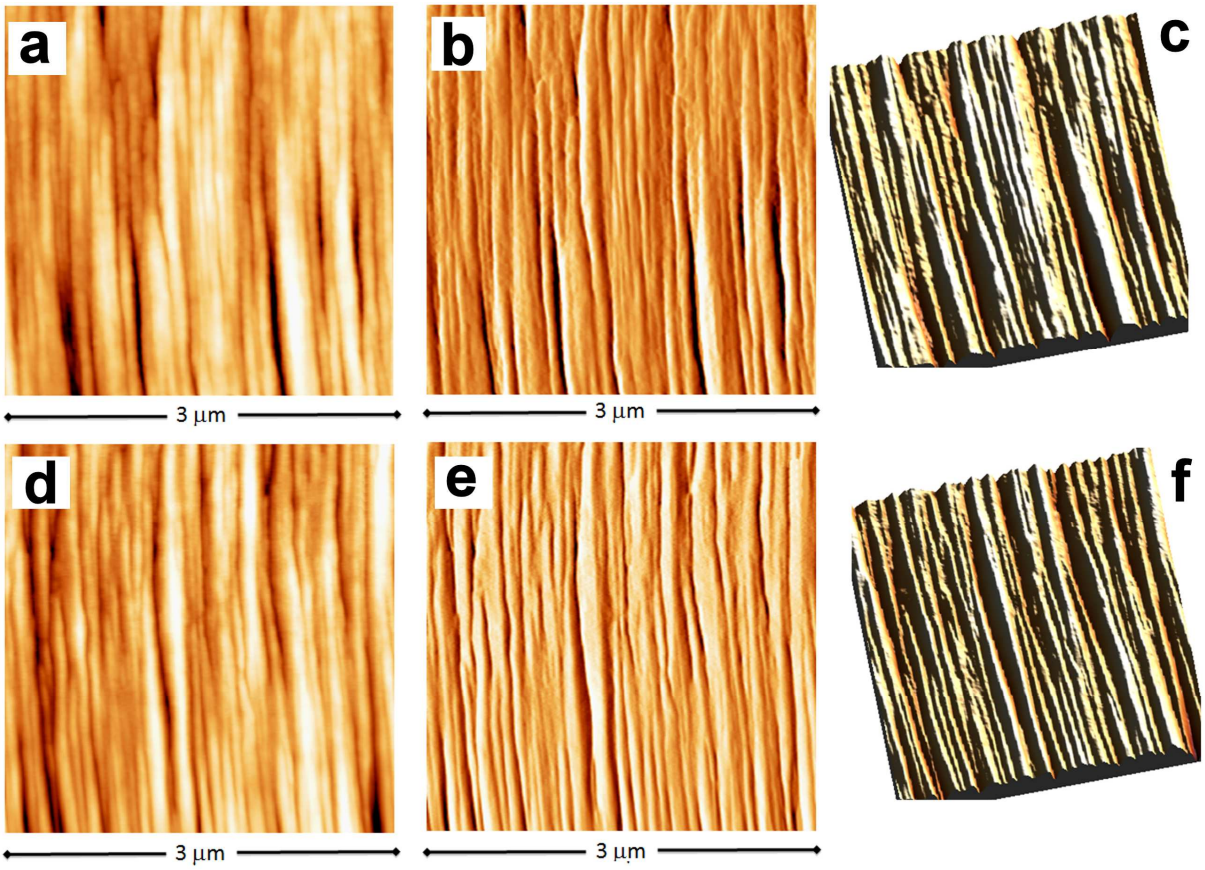

Figure S1: AFM topographies (a, d) acquired on two different sample points. (b, e) Corresponding topography derivative images. (c, f) Corresponding 3D rendering topography images.

2. Methylene Blue probe molecules

We have used Methylene Blue (MB) as a probe molecule for SERS. MB ($C_{16}H_{18}ClN_3S$) is a heterocyclic aromatic chemical compound with many uses in biology[9] and medicine as stain and for photodynamic therapy of cancer.[10, 11, 12, 13] MB is a suitable probe for SERS because of several reasons: (i) the presence of two electron doublets on the sulfur atom fosters the formation of stable chemical bonds of MB with gold and silver substrates on which it adsorbs as a monomer, dimer or as a layer of aggregates;[14, 15] (ii) the monomer has a low fluorescence quantum yield (η = 0.03) while the dimer has no fluorescence;[16] (iii) the presence of delocalized π electrons improves the optical coupling with plasmon modes; (iv) excitation at 633 nm leads to a further resonant

amplification of the Raman emission. At room temperature MB is a solid powder that is soluble in alcoholic solvents, dichloromethane and water. In our experiments MB has been dissolved in deionized (DI) water at a concentration of 10^{-4} M. Binding on the gold nanostructures is achieved by immersion of the metal nanostructures substrate for 45 minutes in the solution and, after rinsing in water, drying in air for 1 hour. During the drying procedure, the glass substrate is held vertically to avoid the formation of droplets that could induce local accumulation of MB.

3. Absorption, Raman and SERS measurements

3.1 Absorption spectroscopy of MB

In aqueous solution, at concentrations of 10^{-4} M, MB molecules appear in monomer or dimer form, with absorption maxima at 670 nm and 620 nm, respectively (Figure S2).[17] Laser excitation at 633 nm yields to Resonant Raman Scattering (RRS) effects and Surface Enhanced Resonant Raman Scattering (SERRS), both providing an amplification of the measured Raman signal.

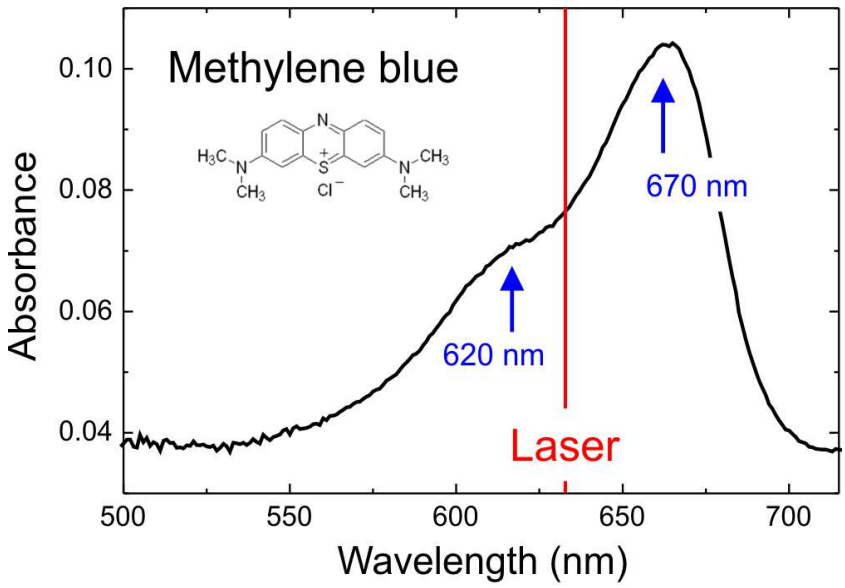

Figure S2: Absorption spectrum of MB aqueous solution at 10^{-4} M. The red vertical line indicates the spectral position of the laser excitation for RRS and SERRS.

3.2 Polarized RRS of MB

Figure S3a shows the Resonant Raman Spectra (RRS) acquired on a drop of a MB solution cast on glass substrate after evaporation of the solvent. Measurements have been acquired on the dense bluish external annular region of the drop, assuring a sufficient concentration to obtain good signal to noise (S/N) ratio even without plasmonic enhancement and using a laser power (50 μW) that does not alter the molecule.

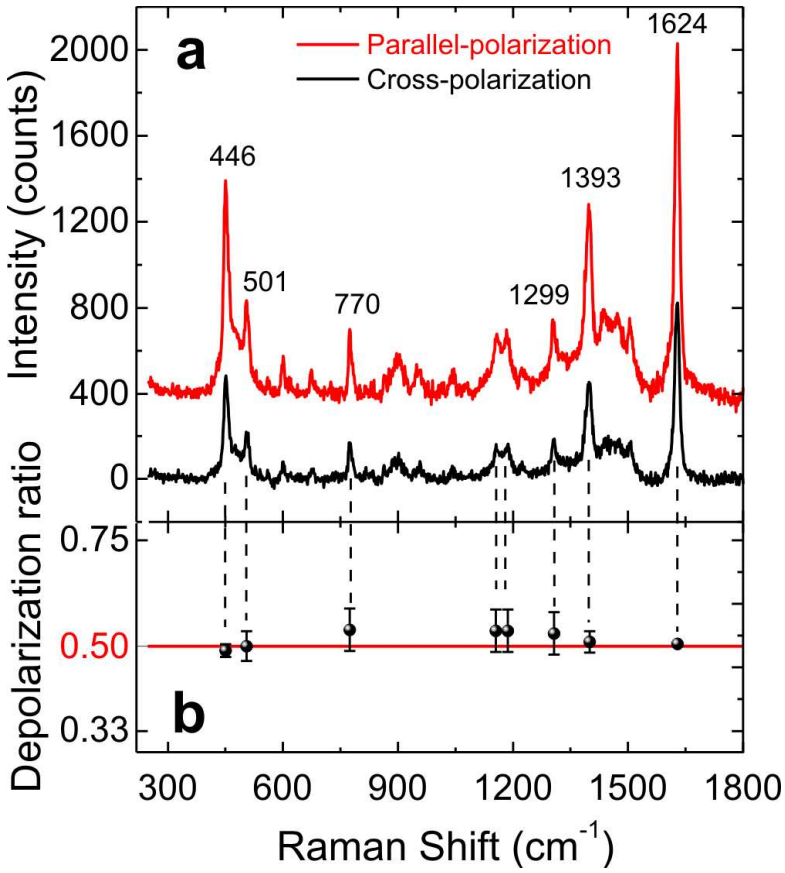

Figure S3: (a) Resonant Raman spectra of MB molecules cast on glass detecting the parallel-polarized (red line) and the cross-polarized (black line) component of the scattering with respect to the laser polarization. Spectra are offset for clarity. Laser power 50 μW, integration time 30sec. (b) Depolarization ratios of the most intense modes.

The spectra (Figure S3a) display the parallel- (red line) and the cross- polarized (black line) components of the Raman scattering. Four major modes, labeled in the figure, are at 446 and 501 cm^{-1} (C-N-C skeleton bending), 1395 cm^{-1} (C-N symmetric stretching), 1624 cm^{-1} (C-C ring stretching).[18], [19] According to ref. 18, the weakness of the peak at 470 cm^{-1} compared to the adjacent modes at 446 and 501 cm^{-1} indicates that MB molecules are mostly dimers. We have experimentally observed that a protracted exposition of MB to the laser light provokes an amplification of the 470 cm^{-1} peak with respect to the adjacent mode at 446 cm^{-1}, together with a decrease of the overall Raman intensity. This result suggests that the intensity of the 470 cm^{-1} peak is in relation with photo-induced damage processes of the molecule. Figure S3b displays that the most intense Raman modes of MB on glass are partially polarized. The 446 cm^{-1} mode, in particular, features a depolarization ratio of $\rho = I_{\perp}/I_{//} = 0.50 \pm 0.03$ Similar values are found for the other major vibrations.

3.3 Polarized SERRS of MB adsorbed on gold nanoparticles.

SERS-active gold nanoparticles substrates have been grown by electron beam evaporation on silica, heating the substrate to 480 °C and evaporating 2-nm-thick Au layer. As shown in the inset of Figure S4, the sample consists of gold nanospheres with diameters ranging from 7 to 25 nm, which form a set of nanocavities (average gap size 5nm) whose axis direction is randomly distributed. The sample features a broad Localized Surface Plasmon Resonance LSPR around 600nm (Figure S4). The SERRS spectra in Figure S5 indicate that we are dealing mostly with dimers of MB molecules since the 470 cm^{-1} peak much is weaker than the adjacent modes at 446 and 501 cm^{-1}.[18] Comparing the cross-polarized component (black line) of the SERRS scattering to the parallel-polarized component (red line) we find a depolarization ratio $\rho = I_{\perp}/I_{//} \cong 0.34 \pm 0.02$ which is exactly what is expected for randomly oriented molecules adsorbed on a set of randomly oriented nanocavities.

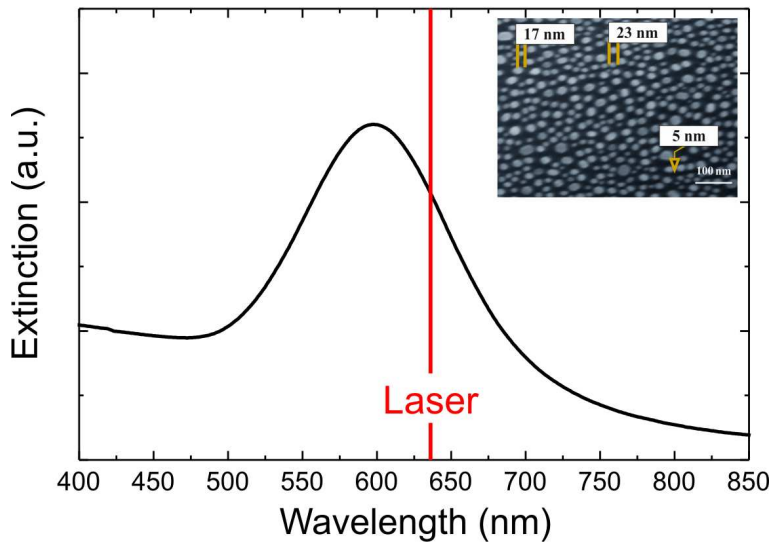

Figure S4: Extinction spectrum of gold nanospheres on silica. The red vertical line indicates the position of the excitation wavelength for SERRS. Inset: Scanning Electron Microscopy image.

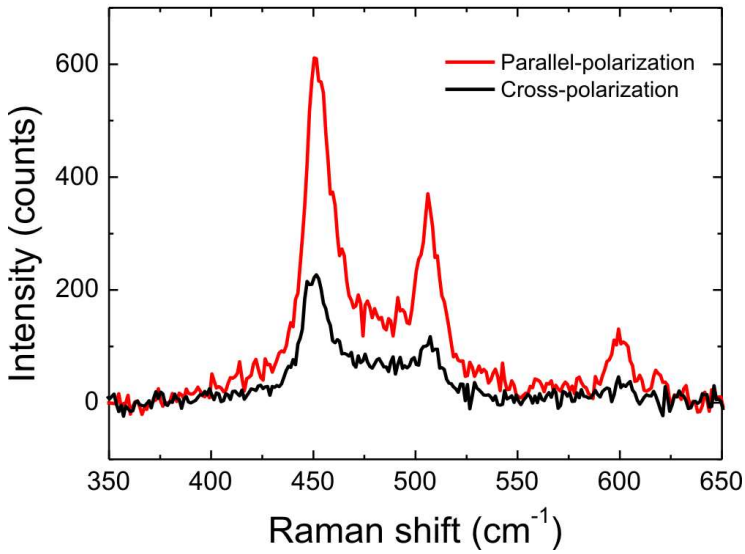

Figure S5: Polarized SERRS spectra of MB adsorbed on gold nanospheres. The parallel-polarized scattering (red line) is 3 times more intense than the cross-polarized component (black line). Excitation laser power is 0.8 μW, integration time is 60s.

3.4 Polarized SERRS of MB adsorbed on gold nanowires

pSERRS measurements on gold NWs have been performed with laser power set to ~ 80 μW and integration time limited to 30s. These parameters minimize the laser-induced damaging of the MB molecules, still providing a good signal to noise ratio. In these conditions we find that two consecutive spectra acquired on the same spot show a signal decrease of less than 5%, at worst. To avoid the summation of this effect, pSERRS spectra have been acquired on random locations of the sample, distant a few tens of microns from each other. Since the laser spot has a diameter of ~ 600nm, each spectrum probes ~ 5-6 nanowires. Unpolarized, parallel- and cross- polarized SERRS measurements have been carried out by rotating the sample with respect to the laser field polarization, while keeping the analyzer angle ϕ fixed at 0° (parallel-polarized SERRS) or 90° (cross-polarized SERRS) with respect to the laser field. This procedure avoids any continuous re-adjustments of the analyzer's angle to follow the laser polarization (the error on ϕ is 5°) and, since ϕ is unchanged, renders the measurements independent from any polarization-dependent response of the spectrometer gratings. The polarizer was removed for the unpolarized measurements.

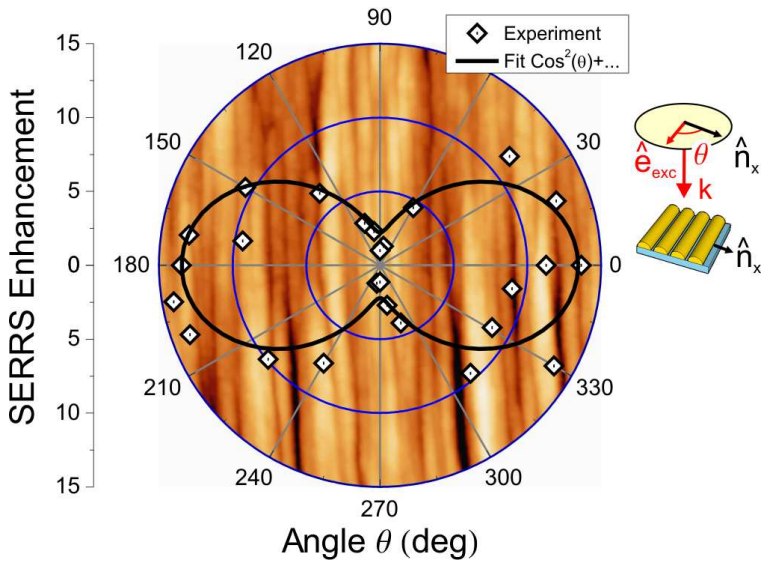

Figure S6: (symbols) Polar plot of the unpolarized SERRS intensity of the 446 cm^{-1} mode Vs the excitation polarization angle θ. The black line is a fit of the data using a $\cos^2\theta$ plus lower order terms model.

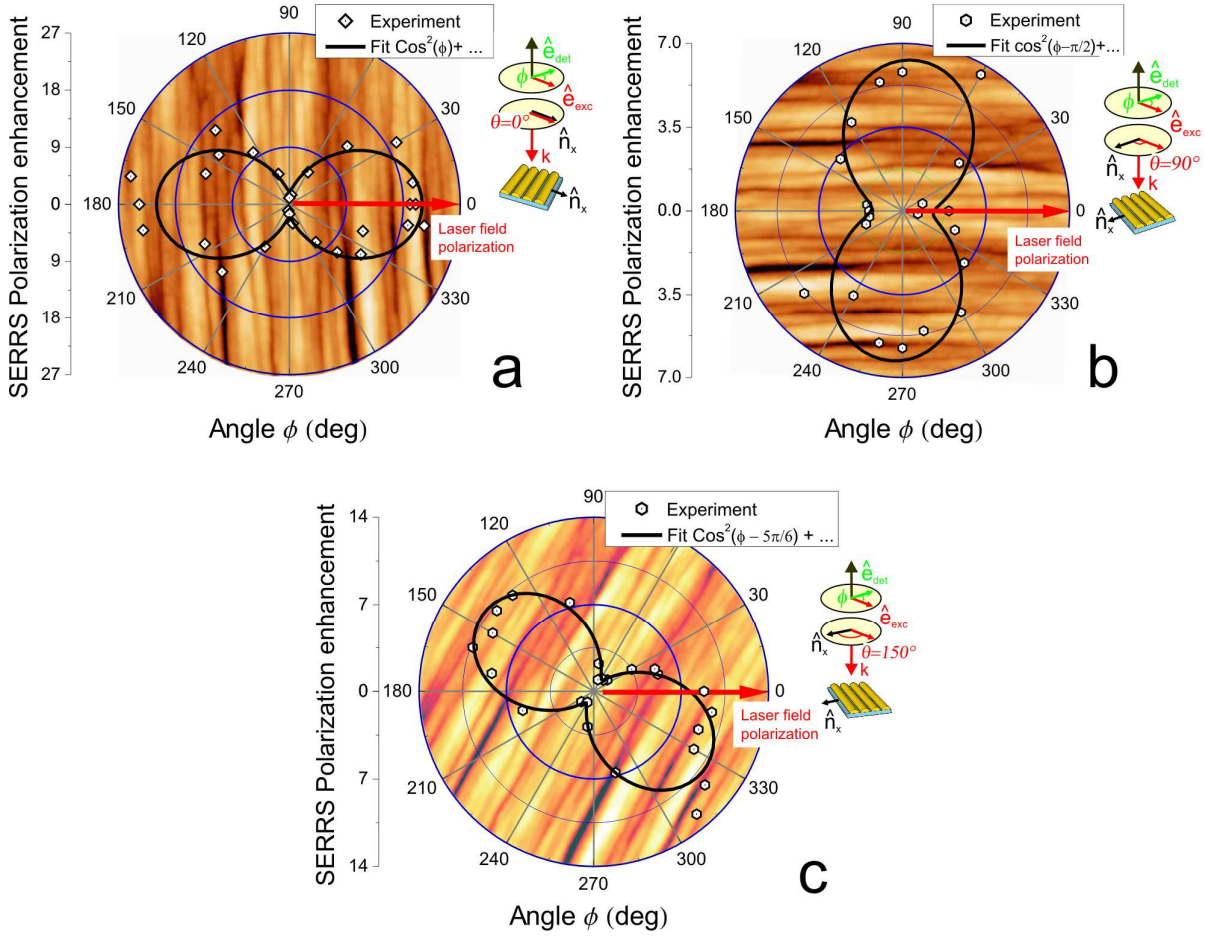

Figure S7: Polar plots of the SERRS polarization enhancement for excitation fields (red arrows) polarized at an angle $\bar{\theta} = 0°$ (a), $\bar{\theta} = 90°$ (b) and $\bar{\theta} = 150°$ (c) with respect to the nanocavity axis $\hat{\mathbf{n}}_x$. The black lines are fits using a $\cos^2(\phi - \bar{\theta})$ plus lower order terms model.

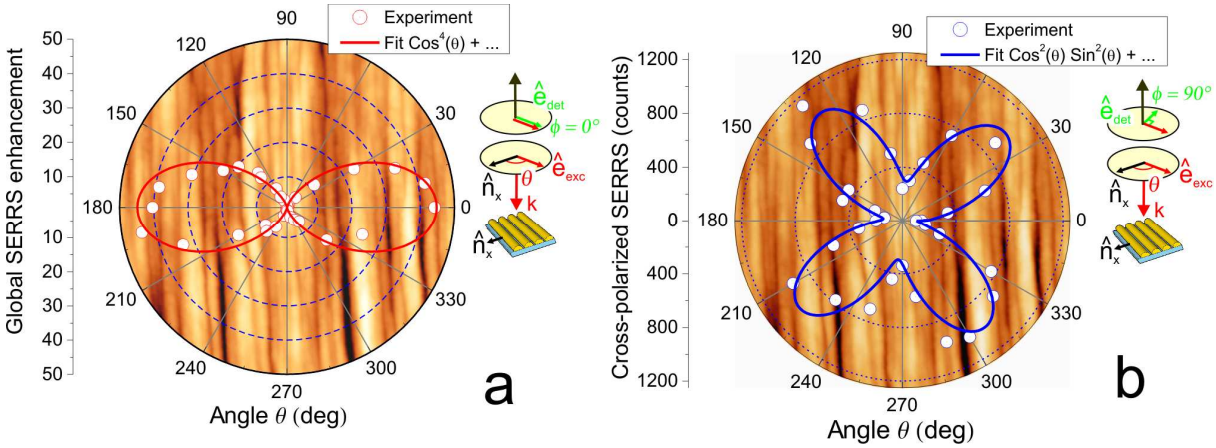

Figure S8: (white symbols) Polar plots of (a) the parallel-polarized $I^{//}_{SERRS}(\theta)$ and of (b) the cross-polarized $I^{\perp}_{SERRS}(\theta)$ SERRS intensities. Data are fitted with a $\cos^4\theta$ (a, red line) and a $\cos^2\theta \cdot \sin^2\theta$ (b, blue line) laws plus lower order terms.

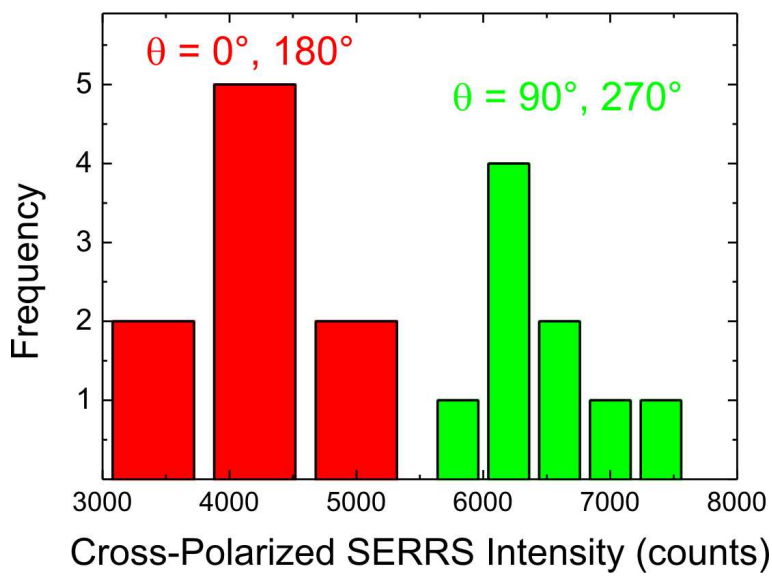

Figure S9: Statistical distribution of the cross-polarized $I^{\perp}_{SERRS}(\theta)$ intensity minima for $\theta = 0°, 180°$ (red) and $\theta = 90°, 270°$ (green) measured from a set of 18 spectra acquired on different points of the sample.

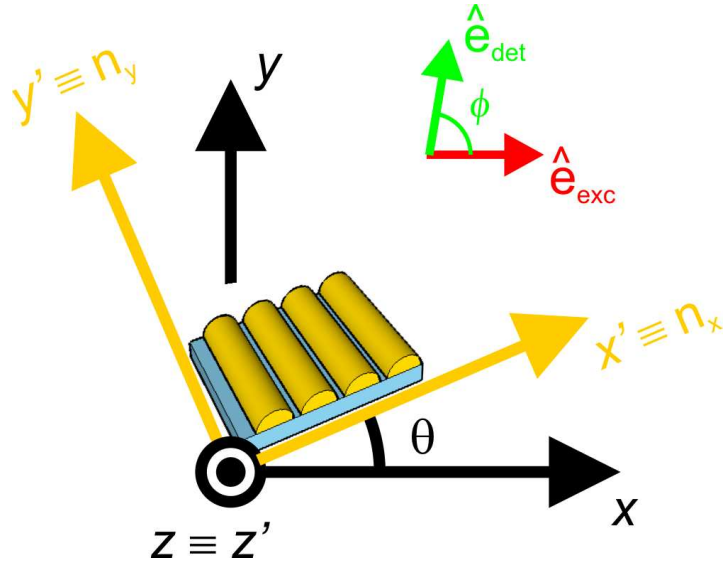

Figure S10: Schematics of the reference frames used for the theoretical calculations. {*x,y,z*} is the laboratory reference frame in which the laser field $\hat{\mathbf{e}}_{exc}$ is polarized along *x*. {*x',y',z'*} is the nanowires reference frame with $\hat{\mathbf{x}}' // \hat{\mathbf{n}}_x$, $\hat{\mathbf{y}}' // \hat{\mathbf{n}}_y$. We call θ the angle between the laser field polarization $\hat{\mathbf{e}}_{exc}$ and the nanocavity direction $\hat{\mathbf{n}}_x$. We call ϕ the angle between the excitation field $\hat{\mathbf{e}}_{exc}$ and the SERS field $\hat{\mathbf{e}}_{\det}$.

3.5 Maximum depolarization ratio for randomly oriented molecules.

For linearly polarized incident light, in the backscattering configuration, the depolarization ratio is defined as the ratio $\rho = I_{\perp}/I_{//}$ between the Raman scattering, $I_{\perp}$, polarized orthogonally to the pump field, and the component $I_{//}$ polarized parallel to the pump field.[20] Conventionally a Raman line is said to be completely polarized when ρ=0, partially polarized when 0<ρ<3/4, depolarized if ρ = 3/4. For randomly oriented molecules the depolarization ratio is a constant strictly related to the orientation-averaged Raman polarizability tensor components of each specific mode, α_{ij}^{υ}, at frequency ν, given by the relation:[20]

$$\rho_{\upsilon} = \frac{\left\langle \left(\alpha_{ij}^{\upsilon}\right)^2 \right\rangle}{\left\langle \left(\alpha_{ii}^{\upsilon}\right)^2 \right\rangle} \tag{S1}$$

where $i,j = x,y,z$, α_{ii}^{υ} are the diagonal components and α_{ij}^{υ} are the off-diagonal components. Moreover, ρ can be expressed through the invariants a (mean polarizability), δ (antisymmetric anisotropy), and γ (anisotropy) as detailed in appendix 14 of ref. 20:

$$\rho = \frac{3\gamma^2}{45a^2 + 4\gamma^2} \tag{S2}$$

Equation S2 shows that for randomly oriented molecules $0 \leq \rho \leq 3/4$.

3.6 Checks on the theoretical model of the Polarization dependence of the SERS signal.

Some checks on the theoretical model can be performed by inspecting the form taken by the equations 5-7 in absence of any enhancement ($\Gamma = 1$, $\varepsilon = 0$). Equations 6 and 7 reduce to the classical formula for the polarized Raman scattering from randomly oriented molecules in backscattering $I_{RS}(\phi) \propto \left\langle \alpha_{ii}^2 \right\rangle \cos^2\phi + \left\langle \alpha_{ij}^2 \right\rangle \sin^2\phi$.[20] Note that, in absence of any symmetry-break induced by the nanoantennas anisotropy, all the laser field polarization directions (angle θ) are equivalent and therefore the Raman intensity is not expected to depend on θ, as it is found. Equations 5 reduce to $I_{RS}^{//} = \left\langle \alpha_{ii}^2 \right\rangle$ and $I_{RS}^{\perp} = \left\langle \alpha_{ij}^2 \right\rangle$ giving the classical expression for the depolarization ratio $\rho = I_{RS}^{\perp} / I_{RS}^{//} = \left\langle \alpha_{ij}^2 \right\rangle / \left\langle \alpha_{ii}^2 \right\rangle$ (see Equation S1). [20] The unpolarized intensity, Equation 7, in absence of enhancement reduces to $I_{RS}^{unpol} = \left\langle \alpha_{ij}^2 \right\rangle + \left\langle \alpha_{ii}^2 \right\rangle$, in agreement with ref. [20] This expression can also be viewed as a suitable comparison term to evaluate the SERS enhancement on randomly oriented molecules. Calculating the SERS enhancement as

$\Gamma_{SERRS} = I_{SERRS}^{unpol}\Big|_{\theta=0^\circ} \Big/ I_{RS}^{unpol}$, for $\Gamma^2 >> 1$, we find in fact $\Gamma_{SERRS} \approx [1/(1+\rho)] \times \Gamma^4 (1+\varepsilon)^2$. This formula is in agreement with ref.[21] and correctly approximates the expected enhancement factor $\Gamma^4 (1+\varepsilon)^2$, since $1/(1+\rho) \approx 1$ because $\rho = 3\gamma^2 / (45a^2 + 4\gamma^2)$ is bound between $0 \le \rho \le 3/4$ (Equation S2).[20]

3.7 Polarized SERS from trimers.

To calculate the polarized response from NPs trimers we adopt the same geometry and the same enhancement tensors assumed in Ref.[22] (see respectively Fig. S1 and Eqs. 2, 3of the same article). The excitation and re-radiation enhancement tensors are

$$\overleftrightarrow{\mathbf{\Gamma}}_{\text{exc}}(\lambda_L) = \begin{pmatrix} 0 & 0 & 0 \\ g_{yx} e^{-i\phi_x} & g_{yy} e^{-i\phi_y} & 0 \\ 0 & 0 & 1 \end{pmatrix} \qquad \overleftrightarrow{\mathbf{\Gamma}}_{\text{rad}}(\lambda_R) = \begin{pmatrix} 0 & g'_{yx} e^{-i\phi'_x} & 0 \\ 0 & g'_{yy} e^{-i\phi'_y} & 0 \\ 0 & 0 & 1 \end{pmatrix} \tag{S3}$$

where $g_{yx}, g_{yy}, g'_{yx}, g'_{yy}$ are the real values and ϕ_x, ϕ_y, ϕ'_x, ϕ'_y are the phases of the tensors elements. The laser field is rotated of an angle θ with respect to the x axis. We introduce the SERS polarization analyzer at an angle ϕ with respect to the laser field. We adopt a generic Raman tensor form (Eq. 10 in the main text) for the molecular vibration considered. Since we work with one single molecule the SERS intensity is $I_{SERS}(\theta,\phi) = \left|\vec{\boldsymbol{\mu}}_{enh} . \hat{\mathbf{e}}_{\text{det}}\right|^2$ or, more explicitly

$$I_{SERS}(\theta,\phi) = \left| \hat{\mathbf{e}}_{\text{det}} \cdot \overleftrightarrow{\mathbf{R}}_z(\theta) \cdot \overleftrightarrow{\mathbf{\Gamma}}_{rad}(\lambda_R) \cdot \vec{\boldsymbol{\alpha}} \cdot \overleftrightarrow{\mathbf{\Gamma}}_{exc}(\lambda_L) \cdot \overleftrightarrow{\mathbf{R}}_z(-\theta) \cdot \hat{\mathbf{e}}_{exc} \right|^2 \tag{S4}$$

which gives

$$\begin{aligned} I_{SERS}(\theta,\phi) &\propto \alpha^2{}_{yy} \cdot g^2{}_{yy}(1+r^2) \cdot g'^2{}_{yy}(1+r'^2) \times \\ &\times \left[1 + \frac{(r^2-1)\cos 2\theta + 2r\cos\Delta \cdot \sin 2\theta}{1+r^2} \right] \cdot \left[1 + \frac{(r'^2-1)\cos 2(\theta+\phi) + 2r'\cos\Delta' \cdot \sin 2(\theta+\phi)}{1+r'^2} \right] \end{aligned} \tag{S5}$$

where $r = g_{yx}/g_{xx}$, $r' = g'_{yx}/g'_{xx}$, $\Delta = \phi_x - \phi_y$, $\Delta' = \phi'_x - \phi'_y$, as in Ref. [22]

From Eq. S5 we find for the total intensity

$$I_{SERRS}^{unpol}(\theta) = I_{SERRS}^{//}(\theta) + I_{SERRS}^{\perp}(\theta) =$$
$$= \alpha^2{}_{yy} \cdot g^2{}_{yy}\left(1+r^2\right) \cdot g'^2{}_{yy}\left(1+r'^2\right) \times \left[1 + \frac{\left(r^2-1\right)\cos 2\theta + 2r \cdot \cos\Delta \cdot \sin 2\theta}{1+r^2}\right] \tag{S6}$$

and for the depolarization factor

$$D(\theta) = \frac{I_{SERRS}^{//}(\theta) - I_{SERRS}^{\perp}(\theta)}{I_{SERRS}^{//}(\theta) + I_{SERRS}^{\perp}(\theta)} = \frac{\left(r'^2-1\right)\cos 2\theta + 2r' \cdot \cos\Delta' \cdot \sin 2\theta}{1+r'^2} \tag{S7}$$

which coincide with eqs. 4 and 5 in Ref. [22]

Indeed both Eqs. S6 and S7 do depend on r and Δ. Since these two parameters are wavelength dependent, as shown by Ref. [22], we indirectly recover the polarization rotation induced by a change of wavelength.

REFERENCES

[1] Rusponi, S.; Costantini, G.; Buatier-de-Mongeot, F.; Boragno, C.; Valbusa U. Patterning a Surface on the Nanometric Scale by Ion Sputtering. *Appl. Phys. Lett.* **1999**, 75, 3318

[2] Valbusa, U.; Boragno, C.; Buatier de Mongeot, F. Nanostructuring Surfaces by Ion Sputtering. *J. Phys.: Condens. Matter* **2002**, 14, 8153–8175.

[3] Murphy, C. J.; Sau, T. K.; Gole, A. M.; Orendorff, C. J.; Gao, J.; Gou, L.; Hunyadi, S. E.; Li, T. Anisotropic Metal Nanoparticles: Synthesis, Assembly, and Optical Applications. *J. Phys. Chem. B* **2005**, 109, 13857-13870.

[4] Kim, F.; Song, J. H.; Yang, P. Photochemical Synthesis of Gold Nanorods. *J. Am. Chem. Soc.* **2002**, 124, 14316-14317.

[5] Laurent, G.; Félidj, N.; Aubard, J.; Lévi, G.; Krenn, J.; Hohenau, A.; Schider, G.; Leitner, A.; Aussenegg, F. Evidence of Multipolar Excitations in Surface Enhanced Raman Scattering. *Phys. Rev. B.* **2005**, 71, 045430.

[6] Toma, A.; Chiappe, D.; Massab, D.; Boragno, C.; Buatier De Mongeot, F. Self-organized Metal Nanowire Arrays with Tunable Optical Anisotropy. *Appl. Phys. Lett.* **2008**, 93, 163104

[7] Belardini, A.; Larciprete, M.C.; Centini, M.; Fazio, E.; Sibilia, C.; Bertolotti, M.; Toma, A.; Chiappe, D.; de Mongeot, F.B. Tailored Second Harmonic Generation from Self-organized Metal Nano-wires Arrays. *Opt. Express* **2009**, 17, 3603

[8] Toma, A.; Chiappe, D.; Šetina Batič, B.; Godec, M.; Jenko, M.; Buatier de Mongeot, F. Erosive versus Shadowing Instabilities in the Self-organized Ion Patterning of Polycrystalline Metal Films. *Phys. Rev. B* **2008**, 78, 153406

[9] Nelson, D. L.; Cox, M. M.; *Lehninger Principles of Biochemistry*, 3rd ed., W. H. Freeman & Co; New York, 2000

[10] Tang, W.; Xu, H.; Kopelman, R.; Philibert, M. A. Photodynamic Characterization and In Vitro Application of Methylene Blue-Containing Nanoparticle Platforms. *Photochem. Photobiol.* **2005**, 81, 242

[11] Johnson, B. E.; Ferguson, J. Drug and Chemical Photosensitivity *Semin. Dermatol.* **1990**, 9, 39

[12] Jockush, S.; Lee, D.; Turro, N. J.; Leonard, E. F. Photo-Induced Inactivation of Viruses: Adsorption of Methylene Blue, Thionine, and Thiopyronine on Qbeta Bacteriophage. *Proc. Natl. Acad. Sci. U.S.A.* **1996**, 93, 7446

[13] Palit, D., Moulik, S. P. Adsorption of the Dyes (Methylene Blue and Acridine Orange and their Mixtures) from Aqueous Solutions on Cholesterol Surface *Colloid J.* **2003**, 65, 350

[14] Spencer, W.; Sutter, J.R. Kinetic Study of the Monomer-Dimer Equilibrium of Methylene Blue in Aqueous Solution. *J. Phys. Chem.* **1979**, 83, 1573

[15] Nicolai, S. H. A.; Rubim, J. C. Surface-Enhanced Resonance Raman (SERR) Spectra of Methylene Blue Adsorbed on a Silver Electrode *Langmuir* **2003**, 19, 4291-4294

[16] Atherton, S. J.; Harriman, A. Photochemistry of Intercalated Methylene Blue: Photoinduced Hydrogen Atom Abstraction from Guanine and Adenine. *J. Am. Chem Soc.* **1993**, 115, 1816-1822

[17] Jockusch, S.; Turro, N. J.; Tomalia, D. A. Aggregation of Methylene Blue Adsorbed on Starburst Dendrimers. *Macromolecules* **1995**, 28, 7416-7418.

[18] Naujok R. R.; Duevel R. V.; Corn R. M. Fluorescence and Fourier Transform Surface-Enhanced Raman Scattering Measurements of Methylene Blue Adsorbed onto a Sulfur-Modified Gold Electrode. *Langmuir* **1993**, 9, 1771-1774.

[19] Tognalli, N. G.; Fainstein, A.; Vericat, C.; Vela, M. E.; Salvarezza, R. C. In Situ Raman Spectroscopy of Redox Species Confined in Self-Assembled Molecular Films. *J. Phys. Chem. C* **2008**, 112, 3741-3746

[20] Long, D. *The Raman Effect*, Wiley, 2002.

[21] Le Ru, E. C.; Meyer, M.; Blackie, E.; Etchegoin, P. G. Advanced Aspects of Electromagnetic SERS Enhancement Factors at a Hot Spot. *J. Raman Spectrosc.* **2008**, 39, 1127-1134

22 Shegai, T.; Li, Z.; Dadosh, T.; Zhang, Z.; Xu, H.; Haran, G. Managing Light Polarization via Plasmon-Molecule Interactions within an Asymmetric Metal Nanoparticle Trimer. *Proc. Natl. Acad. Sci. U.S.A.* **2008**, 105, 16448-16453.